Networked-oscillator-based modeling and control of unsteady wake flows

Aditya G. Nair,[1,*] Steven L. Brunton,[2] and Kunihiko Taira[1]
[1]*Department of Mechanical Engineering, Florida State University, Tallahassee, Florida 32310, USA*
[2]*Department of Mechanical Engineering, University of Washington, Seattle, Washington 98195, USA*

(Received 30 November 2017; published 18 June 2018)

A networked-oscillator-based analysis is performed to examine and control the transfer of kinetic energy for periodic bluff body flows. The dynamics of energy fluctuations in the flow field are described by a set of oscillators defined by conjugate pairs of spatial proper orthogonal decomposition (POD) modes. To extract the network of interactions among oscillators, impulse responses of the oscillators to amplitude and phase perturbations are tracked. Tracking small energy inputs and using linear regression, a networked-oscillator model is constructed that reveals energy exchange among the modes. The model captures the nonlinear interactions among the modal oscillators through a linear approximation. A large collection of system responses is aggregated to capture the general network structure of oscillator interactions. The present networked-oscillator model describes the modal perturbation dynamics more accurately than the empirical Galerkin reduced-order model. The linear network model for nonlinear dynamics is subsequently utilized to design a model-based feedback controller. The controller suppresses the modal amplitudes that result in wake unsteadiness leading to drag reduction. The strength of the proposed approach is demonstrated for a canonical example of two-dimensional unsteady flow over a circular cylinder. The present formulation enables the characterization of modal interactions to control fundamental energy transfers in unsteady bluff body flows.

DOI: 10.1103/PhysRevE.97.063107

I. INTRODUCTION

Oscillations play an important role in a variety of physical and biological systems. These oscillations often result from a set of fluctuating entities called oscillators. Biological oscillators, including neurons and heart cells, are integral to the various rhythms and regulatory systems of the human body. Such collective rhythms arise from the coupling of multiple oscillators with the physics encapsulated by the transfer of energy between them. There has been a rich history of studies on the collective dynamics of oscillators, in particular by Kuramoto [1] and Strogatz [2]. The foundational work laid out by Kuramoto [3] elegantly describes the interactive phase dynamics between oscillators. Mutual synchronization of a system occurs when interacting oscillators affect their phases so as to spontaneously lock on to a particular frequency or phase [4]. The collective phase sensitivity of globally coupled oscillators to external perturbations was investigated by Kawamura *et al.* [5]. In the works of Aizawa [6] and Mirollo and Strogatz [7], the oscillator phase interactions were generalized to incorporate amplitude variation effects. Yamaguchi and Shimizu [8] discovered the amplitude death phenomenon associated with coupled oscillators leading to suppression of oscillator amplitudes to steady state. In the present paper, we examine the coupled oscillator dynamics in unsteady fluid flows.

Unsteady fluid flows governed by the Navier-Stokes equation exhibit strong nonlinear dynamics and are characterized by spatiotemporal oscillations. In flows past bluff bodies, oscillatory behavior of the flows is revealed through shedding of coherent vortices observed in the wake. Such periodic shedding generates unsteady forces on the body which can lead to detrimental increase in drag associated structural fatigue due to the emergence of flow-induced vibrations [9,10]. In the work of Roshko [11], the relationship between form drag and vortex shedding was explored in detail. It was demonstrated that unsteady force oscillations and drag can be reduced by mitigating the wake unsteadiness. Since then, a myriad of studies using active and passive flow control strategies have focused on controlling bluff body wake vortex shedding and the resulting unsteady forces, summarized in a review by Choi *et al.* [12]. Although there have been tremendous breakthroughs in applying flow control techniques for drag reduction, only a few studies make use of the fundamental energy transfer mechanisms and interactions in unsteady fluid flows and controlling the flow unsteadiness therein. Also, suppression of these oscillations is intrinsically associated to the amplitude death phenomena by modification of coupling interactions [13,14].

The oscillations embedded in fluid flows can be extracted naturally as spatial structures (modes) and their associated temporal weights using modal decomposition techniques [15]. For time-periodic flows, individual coherent structures are described by conjugate mode pairs which can be viewed as a set of modal oscillators exhibiting periodic fluctuations. In particular, proper orthogonal decomposition (POD) [16–18] and dynamic mode decomposition (DMD) [19–21] techniques can extract modal oscillators from snapshot flow field data based on energy and dynamics of the flow, respectively. The general behavior of nonlinear flows can also be described by spectral analysis of the linear, infinite-dimensional Koopman

*agn13@my.fsu.edu

operator which yields Koopman modes [20,22,23] closely related to DMD.

The interactions between the modes in unsteady fluid flows can be captured by reduced-order models while dramatically reducing the computational expense to model fluid flows of interest [17,24]. The projection of the Navier-Stokes equations onto the modal basis results in an empirical Galerkin formulation [25]. However, mode deformations and truncation of energy cascades in unsteady fluid flows pose a significant challenge in developing accurate reduced-order models [26,27]. In the current paper, we examine how modal oscillators in unsteady fluid flows interact to distribute energy in unsteady conditions. The present model is constructed by tracking perturbations introduced to the modal oscillators and analyzing the resulting energy transfer dynamics.

The mathematical framework to describe a graph $\boldsymbol{G} = \{\mathcal{V},\mathcal{E},\mathcal{W}\}$ consists of a set of nodes $\mathcal{V}$ connected by edges $\mathcal{E}$ with associated edge weights $\mathcal{W}$ [28,29]. The network nodes form the quantities of interest with the interactions between them as edges. Network analysis is primarily concerned with interactions between quantities of interest [28,30] and has found widespread applications in social sciences [31], biological sciences [32–35], and many other fields [36]. In epidemiology, network analysis has aided in analyzing epidemics and designing appropriate containment and control measures [37–39].

The application of network analysis has recently been extended to represent vortical interactions in fluid flows [40]. The network-theoretic framework is composed of discrete point vortices as nodes and interactions between them as edges. The network representation allows for the utilization of techniques such as spectral sparsification [41] to identify key vortical interactions and development of *sparsified-dynamics* models, which preserve the invariants of discrete vortex dynamics. Moreover, the extraction of the vortical network structure of turbulent flows has revealed the scale-free network property of decaying two-dimensional isotropic turbulence [42]. The resulting framework enables the assessment of the resilience of turbulent flow structures. In the present paper, we extend network analysis to describe and control *modal interactions in fluid flows*, by casting fluid flow in terms of a networked-oscillator system. Here, we view the modal oscillators as nodes and coupling interactions between them as edges, highlighting complex energy transfer dynamics. We utilize modal decomposition techniques in conjunction with coupled oscillator models to capture the interactive physics involved in unsteady fluid flows.

The objective of the present paper is threefold: (1) characterize the nonlinear energy transfer between modes and construct a networked dynamics model for tracking amplitude and phase perturbations in unsteady fluid flows, (2) describe interactive dynamics between modes from a network-theoretic perspective, and (3) control the perturbations with respect to the limit cycle state of periodic flows as well as the full state itself. To accomplish these goals, mode pairs describing individual coherent structures in baseline (unforced and unperturbed) time-periodic flows are considered as a set of oscillators. Examining the impulse responses of the oscillators to perturbations, the associated network structure is extracted using a linear regression procedure [43].

A *networked-oscillator* model herein describes the temporal dynamics of modes in unsteady fluid flow with a network structure embedded in it. With the network dynamics model established, we are able to study the amplitude and phase dynamics of coupled oscillators in the presence of perturbations on the modal interaction network [44]. Thus, we arrive at a reduced-order network model using modal oscillators that highlight energy transfer dynamics among the modes which can subsequently be used for the control of flow unsteadiness. We design flow control strategies to suppress modal fluctuations using the network based insights that consequently leads to drag reduction. In what follows, we first lay the theoretical foundation of this paper in Sec. II. We then demonstrate the strength of our approach using a canonical example of two-dimensional cylinder flow in Sec. III. We end the paper with concluding remarks in Sec. IV.

II. FORMULATION

A. Oscillator representation

Let us first consider the baseline case corresponding to time-periodic flow without any forcing or perturbations introduced in the Navier-Stokes equations. The POD technique, also known as Karhunen-Loève decomposition and principal component analysis, can be utilized to extract coherent structures in fluid flows that span a sequence of finite-dimensional subspaces of the full phase space [25]. POD decomposes the data set to capture maximum energy content with minimum number of basis functions or modes. Using the method of snapshots [16] to compute POD modes, the unsteady velocity field $\boldsymbol{u}$ can be approximated by a finite series in terms of a mean (time-averaged) velocity field $\bar{\boldsymbol{u}}$ and N orthonormal spatial POD modes $\boldsymbol{\phi}_j^{\boldsymbol{u}}$ as

$$\boldsymbol{u}(\boldsymbol{x},t) \approx \bar{\boldsymbol{u}}(\boldsymbol{x}) + \sum_{j=1}^{N} a_j(t)\boldsymbol{\phi}_j^{\boldsymbol{u}}(\boldsymbol{x}), \tag{1}$$

where $a_j(t) = \langle \boldsymbol{u}(\boldsymbol{x},t) - \bar{\boldsymbol{u}}(\boldsymbol{x}), \boldsymbol{\phi}_j^{\boldsymbol{u}}(\boldsymbol{x})\rangle$ are the temporal coefficients and $\langle\cdot,\cdot\rangle$ denotes the inner product over the computational domain. The kinetic energy of the fluctuating velocity field is given by $E = \langle \boldsymbol{u}(\boldsymbol{x},t) - \bar{\boldsymbol{u}}(\boldsymbol{x}), \boldsymbol{u}(\boldsymbol{x},t) - \bar{\boldsymbol{u}}(\boldsymbol{x})\rangle/2$. As the temporal fluctuations of the spatial modes are represented by their temporal coefficients, the contribution of the individual modes to the fluctuation kinetic energy is given by $a_j^2/2$, providing a total modal energy of $E \approx \sum_{j=1}^{N} a_j^2/2$. In this paper, we track the variations in the modal fluctuation energy.

We obtain modes in conjugate pairs from POD for time-periodic flows. Each conjugate mode pair, describing periodic coherent structures in the baseline case, defines an oscillator in our analysis. A set of N POD modes results in $M = N/2$ oscillators. Conjugate mode pairs $(\boldsymbol{\phi}_{2j-1}^{\boldsymbol{u}}, \boldsymbol{\phi}_{2j}^{\boldsymbol{u}})$ with temporal coefficients (a_{2j-1}, a_{2j}) can be represented in the complex plane as

$$z_m = a_{2j-1} + i a_{2j} = r_m \exp(i\theta_m), \tag{2}$$

where $m = \mathrm{I},\mathrm{II},\ldots,M$; $j = 1,2,\ldots,N/2$; $r_m = |z_m|$; and $\theta_m = \angle z_m$. Throughout this paper, the oscillators will be numbered by $m \in \{\mathrm{I}, \mathrm{II},\ldots,M\}$ in roman numerals to distinguish from mode numbering, $j \in \{1,2,\ldots,N\}$. Each oscillator m

is associated with a temporal coefficient (z_m) which consists of an odd-number mode with coefficient a_{2j-1} and an even-number mode with coefficient a_{2j}. The temporal coefficient corresponding to the mean flow ($\bar{\boldsymbol{u}}$), $z_0 = 1$. Equivalent to Eq. (1), we can recover the velocity field in terms of oscillators as

$$\boldsymbol{u}(\boldsymbol{x},t) = \bar{\boldsymbol{u}}(\boldsymbol{x}) + \sum_{m=1}^{M} \big\{ \mathrm{Re}[z_m(t)]\boldsymbol{\phi}^{\boldsymbol{u}}_{2m-1}(\boldsymbol{x}) + \mathrm{Im}[z_m(t)]\boldsymbol{\phi}^{\boldsymbol{u}}_{2m}(\boldsymbol{x}) \big\}, \tag{3}$$

where $\mathrm{Re}(z_m)$ and $\mathrm{Im}(z_m)$ represent real and imaginary components of z_m, respectively.

In the baseline case, oscillators follow a natural limit cycle, which is described by the Stuart-Landau equation

$$\dot{z}^b_m = z^b_m\left(\lambda_m - \left|z^b_m\right|^2 + i\Omega^b_m\right) \tag{4}$$

with $z^b_m = r^b_m \exp(i\theta^b_m)$, $\lambda_m = (\overline{r^b_m})^2$, and Ω^b_m is the oscillator frequency, where $\bar{\cdot}$ denotes the time average and superscript b denotes the baseline case. The dynamics of a set of oscillators can be represented by Eq. (4). In our case, we approximate the dynamics of networked conjugate POD mode pairs by the Stuart-Landau equation. The conjugate mode pairs of each oscillator exchange energy among themselves to describe the self-sustaining equilibrium behavior of each coherent structure in an unsteady fluid flow. Similar to the present analysis, the work of Bagheri [45] demonstrates the use of the Stuart-Landau equation to perform multiscale Koopman expansion of the cylinder wake.

To highlight interactions between the oscillators, we introduce perturbations impulsively in direct numerical simulation (DNS) to the baseline temporal coefficients of oscillators at $t = t_0$. These perturbations introduced to the baseline state enable the emergence of nonlinear interactions and energy exchange among the oscillators resulting in fluctuations described by

$$z'_m = a'_{2j-1} + ia'_{2j} = \epsilon'_m r^b_m \exp\left(i\left[\theta^b_m + \theta'_m\right]\right), \tag{5}$$

where $()'$ denotes the perturbation quantity and $\epsilon'_m(t_0)$ and $\theta'_m(t_0)$ are the amplitude and phase perturbations for the mth oscillator, respectively. Note that ϵ'_m is normalized by the baseline amplitude of each oscillator. The energy exchange between the oscillators captures the transfer of fluctuation kinetic energy.

The total temporal coefficient for each oscillator in the perturbed case can then be described by combining the baseline temporal coefficient and fluctuation as

$$z_m = r_m \exp(i\theta_m) = z^b_m + z'_m. \tag{6}$$

The overall oscillator model, including perturbations, is shown in Fig. 1. The blue circle in the top left figure indicates the natural limit cycle for oscillator m (z^b_m). The perturbations in amplitude (ϵ'_m) and phase (θ'_m) result in a total temporal coefficient (z_m) off the limit cycle. Perturbations can be introduced to each oscillator m by specifying the initial amplitude of perturbation $\epsilon'_m(t_0)$ and initial phase perturbation size $\theta'_m(t_0)$. Once these factors are prescribed, using Eqs. (5), (6), and (3), the initial velocity field for DNS is prepared.

Once the perturbations are introduced to the flow, the perturbation energy is distributed among the oscillators according

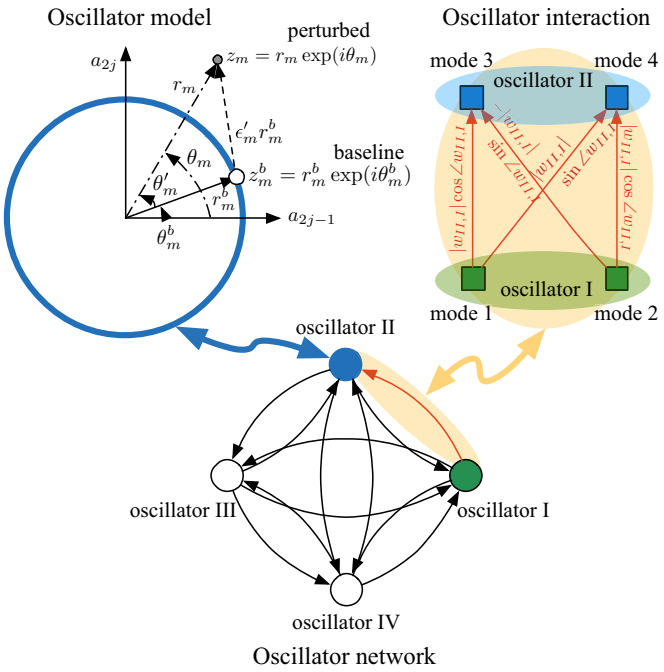

FIG. 1. Modal oscillator model in the complex plane and oscillator network. The circle in the oscillator model describes the limit cycle trajectory of the oscillators (z^b_m) and the perturbed temporal coefficients (z_m). The nodes of the network correspond to oscillators with directed edges showing interactions. Modal interactions corresponding to edges from oscillator I to II highlighted in red (bottom shaded edge) are further expanded (top right).

to natural advection and diffusion. The temporal dynamics of the modes are attributed to the interactions resulting primarily from the advective term of the Navier-Stokes equation. The temporal coefficients of the modes in the perturbed case can be extracted by projection, as $a_j = \langle \boldsymbol{u} - \bar{\boldsymbol{u}}, \boldsymbol{\phi}^{\boldsymbol{u}}_j \rangle$. We then construct z_m for each oscillator m using Eq. (2). To capture the fluctuating amplitude $\epsilon'_m(t)$ and phase $\theta'_m(t)$ of the temporal coefficients due to interactions, we track the normalized fluctuation

$$\zeta_m = z'_m / z^b_m = \epsilon'_m \exp(i\theta'_m). \tag{7}$$

The amplitude fluctuations of the oscillators are related to the variation in oscillator fluctuation energy $E'_m(t)$ compared to the baseline, given by

$$E'_m = \tfrac{1}{2}\left(|z_m|^2 - \left|z^b_m\right|^2\right) = \tfrac{1}{2}[(1+\epsilon'_m)^2 - 1]\left(r^b_m\right)^2, \tag{8}$$

where $E'_m(t_0)$ represents the oscillator energy input and the total baseline modal energy, $E^b = \sum_{m=1}^{M} (r^b_m)^2/2$. If only phase perturbations are introduced in the simulation, a variation in oscillator energy may be observed due to oscillator interactions, although $E'_m(t_0) = 0$. The quantities $E'_m/(r^b_m)^2$ and θ'_m are used to track the energy perturbations and phase of the oscillators, respectively. The perspective of viewing the flow as an ensemble of limit cycle Stuart-Landau oscillators, each with their own intrinsic frequency, enables a network-based representation of the fluid flow dynamics as discussed below.

B. Networked oscillator representation

Based on the oscillator representation using the POD modes and the fluctuations about the baseline flow, we can now create a network-theoretic representation of the unsteady fluid flow system. We consider the collection of oscillators (modes pairs) characterizing unsteady fluctuations to be the nodes ($\mathcal{V}$) of the network and the interaction between them as edges ($\mathcal{E}$). To characterize the interactions between oscillators, we need a model that captures the coupling between the oscillators. This motivates a networked-oscillator model of M linearly coupled oscillators given by

$$\dot{\zeta}_m = \sum_{n=\mathrm{I}}^{M} [\boldsymbol{A}_{\mathcal{G}}]_{mn}(\zeta_n - \zeta_m) = -\sum_{n=\mathrm{I}}^{M} [\boldsymbol{L}_{\mathcal{G}}]_{mn}\zeta_n, \tag{9}$$

where $[\boldsymbol{A}_{\mathcal{G}}]_{mn}$ and $[\boldsymbol{L}_{\mathcal{G}}]_{mn}$ are the adjacency and the in-degree graph Laplacian matrices, respectively. The dynamics of normalized fluctuations of temporal coefficients are nonlinear in general due to convective physics in unsteady fluid flows.

For a set of M oscillators, the above adjacency matrix $\boldsymbol{A}_{\mathcal{G}} \in \mathbb{C}^{M\times M}$ concisely describes the network connectivity given as

$$[\boldsymbol{A}_{\mathcal{G}}]_{mn} = w_{mn} = |w_{mn}| \exp(i\angle w_{mn}). \tag{10}$$

The rows of the adjacency matrix indicates the dependence of the oscillators n on the dynamics of oscillators in column m, i.e., w_{mn}. The in-degree (k_m) of a node m represents the summation of the incoming weights of the edges connected to it given by $k_m = \sum_{n=\mathrm{I}}^{M} [\boldsymbol{A}_{\mathcal{G}}]_{mn}$. The (in-degree) graph Laplacian is related to the adjacency matrix as $\boldsymbol{L}_{\mathcal{G}} = \boldsymbol{D}_{\mathcal{G}} - \boldsymbol{A}_{\mathcal{G}}$, where $\boldsymbol{D}_{\mathcal{G}}$ is a diagonal matrix with elements equal to the in-degree of the nodes, $\boldsymbol{D}_{\mathcal{G}} = \mathrm{diag}([k_m]_{m=\mathrm{I}}^{M})$. The graph Laplacian is a discrete analog of the continuous Laplacian operator. In the current paper, it encodes structural properties of the networked-oscillator model.

Using the time series of normalized fluctuations of each oscillator from DNS, i.e., $\boldsymbol{\zeta}$ and $\dot{\boldsymbol{\zeta}}$, we use a linear regression procedure to determine the adjacency matrix weights for the networked-oscillator model. These weights could also be obtained through a Galerkin regression approach [46]. The temporal coefficient associated with the mean flow is assumed to be fixed at unity and does not contribute to normalized fluctuations of the modes. Thus, the mean flow is considered as an isolated node in this formulation.

The oscillator network representation is illustrated in Fig. 1. The magnitudes of the edge weights ($|w_{mn}|$) signify the influence of oscillator n on oscillator m as illustrated in Fig. 1. The phase of the edge weights ($\angle w_{mn}$) represents the individual modal contributions in oscillator phase interactions. In particular, it highlights the phase advances or delays imposed between modes of interacting oscillators. The odd-odd mode interactions and even-even mode interactions are given by $|w_{mn}|\cos\angle w_{mn}$ while the odd-even and even-odd mode interactions are given by $|w_{mn}|\sin\angle w_{mn}$ and $-|w_{mn}|\sin\angle w_{mn}$, respectively. Details are provided in the Appendix.

For comparison with the networked-oscillator model, we also consider the Galerkin projection model for the incompressible Navier-Stokes equations, by projecting the equations onto the POD modes to construct the POD-Galerkin reduced-order model [25,47]. The resulting Galerkin model can be expressed as

$$\dot{a}_j = \gamma_j + \sum_{k=1}^{N} \psi_{jk} a_k + \sum_{k,l=1}^{N} \chi_{jkl} a_k a_l, \quad i = 1,2,\ldots N, \tag{11}$$

with

$$\begin{aligned}
\gamma_j &= \frac{1}{\mathrm{Re}}\langle \boldsymbol{\phi}_j, \nabla^2 \bar{\boldsymbol{u}}\rangle - \langle \boldsymbol{\phi}_j, \nabla\cdot(\bar{\boldsymbol{u}}\bar{\boldsymbol{u}})\rangle,\\
\psi_{jk} &= \frac{1}{\mathrm{Re}}\langle \boldsymbol{\phi}_j, \nabla^2 \boldsymbol{\phi}_k\rangle - \langle \boldsymbol{\phi}_j, \nabla\cdot(\bar{\boldsymbol{u}}\boldsymbol{\phi}_k)\rangle - \langle \boldsymbol{\phi}_j, \nabla\cdot(\boldsymbol{\phi}_k\bar{\boldsymbol{u}})\rangle,\\
\chi_{jkl} &= -\langle \boldsymbol{\phi}_j, \nabla\cdot(\boldsymbol{\phi}_k\boldsymbol{\phi}_l)\rangle,
\end{aligned} \tag{12}$$

where γ_j, ψ_{jk}, and χ_{jkl} are the constant mean shift coefficient, linear coefficient, and quadratic coefficient terms, respectively. The linear term represents diffusive physics of the modes, while the quadratic term represents the advective physics.

III. APPLICATION TO FLUID FLOW

We now consider the application of the networked-oscillator approach to the two-dimensional flow over a circular cylinder, which serves as a canonical flow.

A. Computational approach

We gather the flow field data from DNS of incompressible flow past a circular cylinder using the immersed boundary projection method [48–50] at a diameter-based Reynolds number of $\mathrm{Re} = 100$. This method employs a Cartesian grid with the immersed boundary formulation to generate the cylinder. We take advantage of the multidomain technique to simulate cylinder flow in free space. The innermost domain is chosen as $-1 \leqslant x/d \leqslant 29, -15 \leqslant y/d \leqslant 15$ with a resolution of 600×600 grid points where d is the cylinder diameter. Here, x is the streamwise direction and y is the cross-stream direction. The outermost domain is chosen as $-16 \leqslant x/d \leqslant 44, -30 \leqslant y/d \leqslant 30$, far enough so as to not affect the results in the near field. Uniform flow is prescribed at the far-field boundaries. For time integration, this solver uses an implicit Crank-Nicholson scheme for the viscous term and an Adam-Bashforth method for the advective term.

From the simulation, the drag coefficient (C_D) and lift coefficient (C_L) are computed as

$$C_D = \frac{F_D}{\frac{1}{2}\rho U^2 d} \quad \text{and} \quad C_L = \frac{F_L}{\frac{1}{2}\rho U^2 d}, \tag{13}$$

where F_D and F_L are the drag and lift forces on the cylinder, ρ is the freestream density, and U is the freestream velocity field. The Strouhal number for the flow is $\mathrm{St} \equiv f_n d/U$, where f_n is the natural shedding frequency. We obtain a Strouhal number of $\mathrm{St} = 0.164$, drag coefficient $C_D = 1.35 \pm 0.009$, and lift coefficient $C_L = \pm 0.325$ from DNS, which agree well with those reported in the literature [48,51,52]. The flow exhibits vortex shedding behavior in the cylinder wake, as shown by the instantaneous vorticity field in Fig. 2(a). Such vortex shedding characterizes a von Kármán vortex street due to the repetitive pattern of vortices in the unsteady wake. The time-averaged (mean) vorticity field is shown in Fig. 2(b). We collect the snapshots of the flow field and perform POD on the velocity

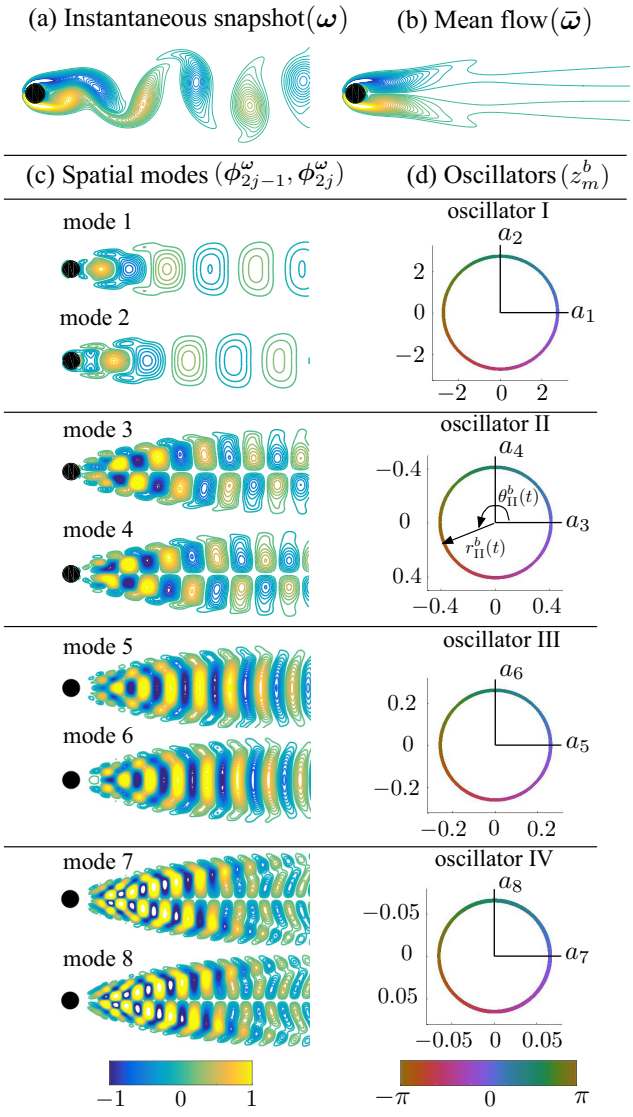

FIG. 2. (a) Instantaneous and (b) time-averaged (mean) vorticity fields. Proper orthogonal decomposition (POD) applied to the cylinder flow problem results in (c) spatial modes and (d) temporal coefficients of oscillators in the complex plane. The colorbar of the spatial modes indicates the contour level and the colorbar of the temporal coefficients and oscillators indicates the phase of the oscillators varying from $[-\pi,\pi]$ over the periodic limit cycles.

field ($\boldsymbol{u}$) with the method of snapshots [16]. The POD modes and temporal coefficients obtained are in agreement with those from the work by Noack *et al.* [24]. The extracted spatial modes in terms of the vorticity field, $\boldsymbol{\phi}^{\boldsymbol{\omega}}_j = \nabla \times \boldsymbol{\phi}^{\boldsymbol{u}}_j$, are shown in Fig. 2(c).

B. Unperturbed flow (baseline)

We define the conjugate mode pairs as independent oscillators in our formulation. The oscillators are ordered in terms of decreasing energy content, shown in Fig. 2 (top to bottom). As the first eight POD modes capture 99.98% of the fluctuation kinetic energy, we choose $N = 8$ for our analysis. The energy content of oscillators I, II, III, and IV are 96.87,2.18,0.88, and 0.05%, respectively. The oscillator temporal coefficients in the complex plane (z^b_m) are shown in Fig. 2(d). For this canonical problem, the frequencies associated with the higher-order oscillators are harmonics of the lowest-order oscillator, $\Omega^b_m = m\Omega^b_{\rm I}$ with $\Omega_{\rm I} = {\rm St} = 0.164$. As the frequency (Ω^b_m) associated with the temporal coefficients of the mode pairs increases, the size of the spatial modal structures becomes finer. Again, the oscillators in the baseline flow are associated with limit cycle temporal dynamics described by Eq. (4). The lack of coupling in the generalized limit cycle dynamics is unable to capture the oscillator interactions in unsteady fluid flow, which calls for the analysis below.

C. Perturbed flow

To capture interactions between oscillators, additional fluctuation energy and phase perturbations are introduced to the simulation through the initial condition. These perturbations cause added fluctuations in the temporal coefficients of the modes. The projected coefficients from the perturbed case are extracted from DNS and the normalized fluctuation $\zeta_m(t)$ is tracked using the networked-oscillator model discussed in Sec. II. We expect that as the perturbation convects downstream, the normalized fluctuation of the oscillators will decay to zero and the perturbed flow will return to the baseline limit cycle. However, the addition of a perturbation to the flow results in a constant phase shift of each oscillator in the final limit cycle, compared to the unperturbed limit cycle.

In two-dimensional unsteady cylinder flow, the leading POD mode pair (oscillator I) holds the largest energy content. Any deviation from the baseline limit cycle is immediately reflected in the phase of oscillator I ($\theta_{\rm I}$). Thus, to construct the normalized fluctuation time series for each oscillator, we align the phase of oscillator I for the perturbed case and the baseline case as $\zeta_m = (z_m - z^b_m|_{\theta=\theta_{\rm I}})/z^b_m|_{\theta=\theta_{\rm I}}$. Once the normalized fluctuation ζ_m is evaluated, we also determine its time derivative $\dot{\zeta}_m$. We then construct the bases $(\zeta_n - \zeta_m)$ for each oscillator m. We perform a simple linear regression on the time series to obtain the network structure $[\boldsymbol{A}_{\mathcal{G}}]_{mn}$. Once the network structure is obtained, we solve the linear networked-oscillator model in Eq. (9) for prediction with a prescribed initial condition and compare the fluctuations with those obtained in DNS. While it is not necessary, one could also consider quadratic or higher interaction terms [46,53].

Let us demonstrate the model development for a case where we first introduce an amplitude perturbation to oscillator II. Addition of a perturbation at this harmonic frequency perturbs not only the natural shedding process but also the oscillators associated with higher harmonics of the flow due to interactions. Let us consider the addition of 20% of baseline modal energy to oscillator II. No perturbation in phase is added, i.e., $\theta'_{\rm II}(t_0) = 0$. As the introduced perturbation in oscillator II convects downstream in the numerical simulation, its energy propagates to other oscillators through interactions. Using the procedure discussed above, we can extract the adjacency matrix $\boldsymbol{A}_{\mathcal{G}}$ that captures network interactions.

The magnitude and phase of the adjacency matrix are shown in Fig. 3(a). In this example, the dynamics of oscillator I is not affected noticeably by the other oscillators. The dynamics of oscillators II and III show strong dependence on oscillator I. This is consistent with our expectation as most of the energy in

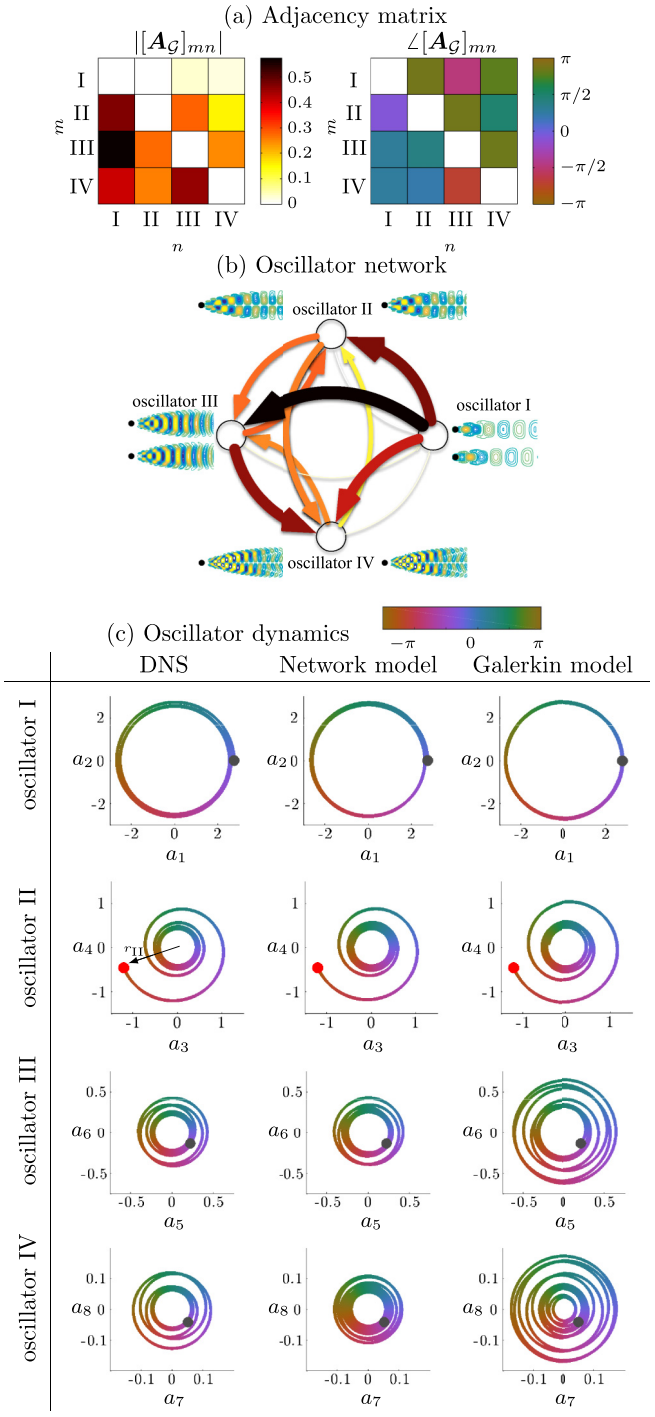

FIG. 3. Response of the system to amplitude perturbation introduced to oscillator II. (a) Adjacency matrix of the networked-oscillator model and (b) corresponding network of oscillator interactions. The color and thickness of the network edges in the network represent the magnitude of the elements of $\boldsymbol{A}_{\mathcal{G}}$. (c) Oscillator dynamics from DNS, the networked-oscillator model, and the POD-Galerkin model (color of temporal dynamics of oscillators indicates phase). The red dot in oscillator II dynamics indicate the initial perturbation.

the flow is held in oscillator I and passes down to higher-order oscillators. For the dynamics of oscillator II (modes 3 and 4), the phase of the edge weights indicates that interactions between modes $1 \rightarrow 3$, $2 \rightarrow 4$, $8 \rightarrow 3$, and $7 \rightarrow 4$ are larger than other modal interactions. For this perturbed case, phase advancing effects are generally predominant for the oscillators affecting each other. The network structure of oscillators is visualized in Fig. 3(b) illustrating the leading influence of oscillator I.

We then solve the linear networked-oscillator model specifying the perturbed initial condition. For comparison, we also prepare the empirical Galerkin reduced-order model. The oscillator dynamics from DNS (reference) and those predicted from the networked-oscillator and POD-Galerkin models are shown in Fig. 3(c). The initial amplitude of the perturbed temporal coefficients for oscillator II ($r_{\mathrm{II}}(t_0)$) corresponds to the red dot. The initial amplitude and phase of the other oscillators are unchanged, as no perturbations are introduced to these oscillators. It can be seen in Fig. 3(c) that the oscillator dynamics predicted by the networked-oscillator model agree well with DNS trajectories, particularly oscillators I, II, and III. Due to its low energy content, any small deviation in the dynamics of lower-order oscillators causes comparable changes in the trajectory of oscillator IV. On the other hand, the POD-Galerkin model overpredicts the fluctuations in oscillators. As discussed in the work by Rempfer [54], the restricted completeness property of the POD basis creates problems for integrating the POD-Galerkin system for any initial conditions lying outside the ensemble of trajectories used to compute the basis. Thus, small perturbations or disturbances created by numerical error in integration of the Galerkin model lead to incomplete representation of the Navier-Stokes operator.

There are two mechanisms of kinetic energy transfers in incompressible fluid flows, one from advection and the other from dissipation. In the incompressible Navier-Stokes equations, the advective term $-(\nabla \cdot \boldsymbol{u})\boldsymbol{u}$ results in advection of kinetic energy in the flow while the diffusion term $\nu\nabla^2\boldsymbol{u}$ results in dissipation of energy [55]. In the Galerkin model, the energy dissipation is modeled by the linear term and the advective energy transfer is modeled by the quadratic term [56]. In the networked-oscillator model, the diagonal terms of the Laplacian contribute to the dissipative physics of the individual oscillators and the off-diagonal terms model the advective physics. The absence of the mean in the network oscillator model results in energy exchanges only between the oscillators.

To further compare the details of the predicted trajectories, we track the fluctuations in modal amplitude and oscillator energy in Fig. 4. The networked-oscillator model shows excellent agreement with DNS, tracking the amplitude (a_{2j-1}) and energy transfers (E'_m). Moreover, we see agreement in the long-time behavior of the fluctuations as the flow returns to the baseline state for the networked-oscillator model. In contrast, the POD-Galerkin model is not well designed for modeling the long-time behavior of modal fluctuations and hence is not expected to work well as time progresses [57,58]. As indicated by the green dashed line, the POD-Galerkin model overpredicts these fluctuations and their associated time scales.

D. Aggregate network model

The network structure of interactions can be extracted individually by tracking the trajectory of the oscillator fluctuations from DNS as demonstrated above. While the

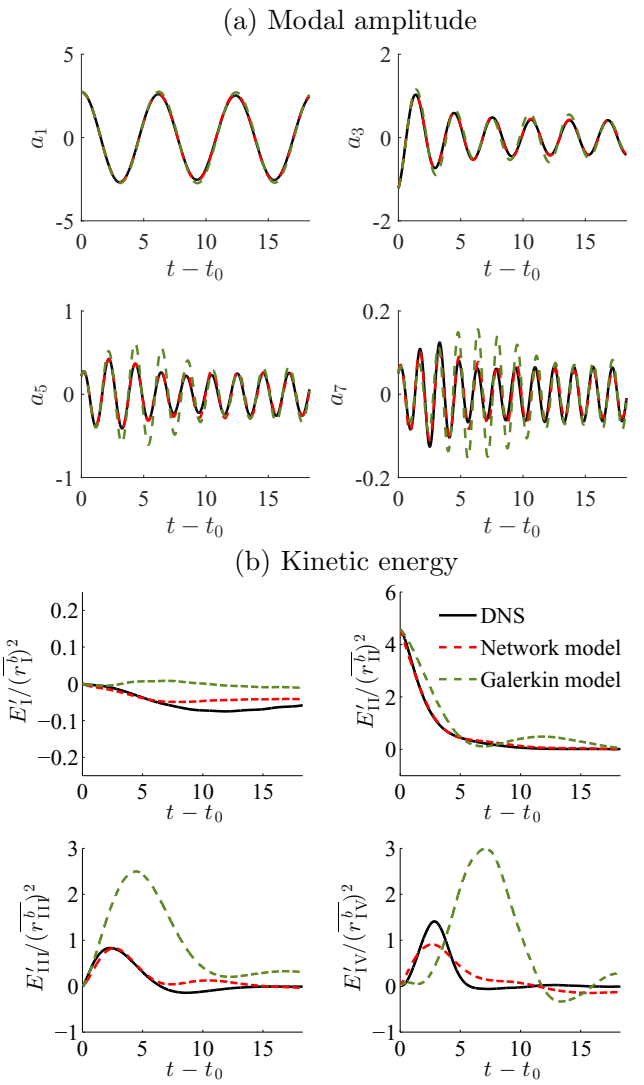

FIG. 4. (a) Modal amplitude and (b) energy tracking for amplitude perturbation introduced to oscillator II. Network model and Galerkin model dynamics are shown by red (darker gray) and green (lighter gray) dashed lines, respectively.

corresponding linear networked-oscillator models can be built for each specific case, the resulting network structure obtained depends on the initial perturbations introduced. Thus, one may argue that such individually tuned models do not necessarily capture the overall interactions in response to a generic perturbation. A general network interaction model is desired not only to capture interactions for any combination of perturbations but also to design effective strategies for flow control. In this section, we describe our approach to build an aggregate network model that captures the fluid flow response to a variety of perturbation inputs.

We consider a range of perturbed flow cases by varying the amplitude and phase of perturbations to different combinations of oscillators. For a particular oscillator perturbed, we vary the energy input from 5 to 100% additional baseline modal fluctuation energy in the flow. We also vary the phase perturbation size (θ'_m) from $-2\pi/3$ to $2\pi/3$ to cover a broad coverage of plausible initial perturbations introduced. The range of amplitude and phase perturbations considered here is quite large. These large perturbations lead to the emergence of strong nonlinear interactions between the oscillators. For the variety of perturbation cases, we collect the oscillator fluctuation data from DNS. To build an aggregate network model, we concatenate the trajectories of all the perturbed cases obtained from DNS instead of individually tracking perturbations and monitoring the oscillator fluctuations in each perturbed case.

We then segregate the collection of data into training and test sets to perform cross-validation and evaluate the predictive capabilities of the network model. Varying fractions of the combined input-output data are randomly chosen as the training sets. For each training set, regression analysis is performed to extract a corresponding network model. We then examine the in-degree ($k_m = \sum_{n=\mathrm{I}}^{M}[\boldsymbol{A}_{\mathcal{G}}]_{mn}$) and out-degree ($k_n = \sum_{m=\mathrm{I}}^{M}[\boldsymbol{A}_{\mathcal{G}}]_{mn}$) of the network nodes for each model extracted. The variation of the network degrees with respect to the fraction of the chosen training set is shown in Fig. 5(a). We observe that, as the fraction of the training data used increases, convergence of the network degree is obtained. We also learn that the average in-degree increases from low-order oscillators to higher-order oscillators and the average out-degree decreases. Oscillators I and IV have maximum out-degree and in-degree, respectively. Oscillator I influences the other oscillators most, while oscillator IV is the most influenced. Oscillators II and III have more balanced in- and out-degrees indicating more balanced energy transfer for each mode.

We observe a convergence of network degree for a fraction of training data, $f_{\mathrm{train}} \geqslant 0.8$. We randomly choose 80% of the combined input-output data as the training set and use the remaining 20% of the data to assess the performance of the network model extracted. Using the training set, the adjacency matrix for the aggregate network model extracted is shown in Fig. 5(b). The magnitude of the network reveals that the lower-order oscillators have more influence on the dynamics of the higher-order oscillators. This follows from our earlier discussion regarding the network node degrees and agrees with our intuition that energy is passed from lower-order oscillators to higher-order oscillators. Alternatively, we can construct the aggregate network model by considering complete trajectories of randomly chosen perturbed cases yielding a very similar aggregate network model.

We also compare the aggregate network model with network models built with selectively chosen training sets. In particular, we consider trajectories of perturbed cases of individual oscillators. Combining the perturbed trajectories for various amplitude and phase perturbation sizes for each oscillator, we build network models corresponding to oscillators I, II, III, and IV. We use the same test data set as before to assess the performance of each of these models along with the aggregate model. We predict the time derivative of the normalized fluctuation $\dot{\zeta}_m$ with each of the models on the test data set and compare with DNS reference values. In Fig. 5(c), we assess the prediction error through a normalized root mean square deviation ($\triangle_m$), given by

$$\triangle_m = \frac{1}{\max(|\dot{\zeta}_m|)}\sqrt{\frac{\sum_{k=1}^{n_t}|\hat{\dot{\zeta}}_m(k) - \dot{\zeta}_m(k)|^2}{n_t}}, \qquad (14)$$

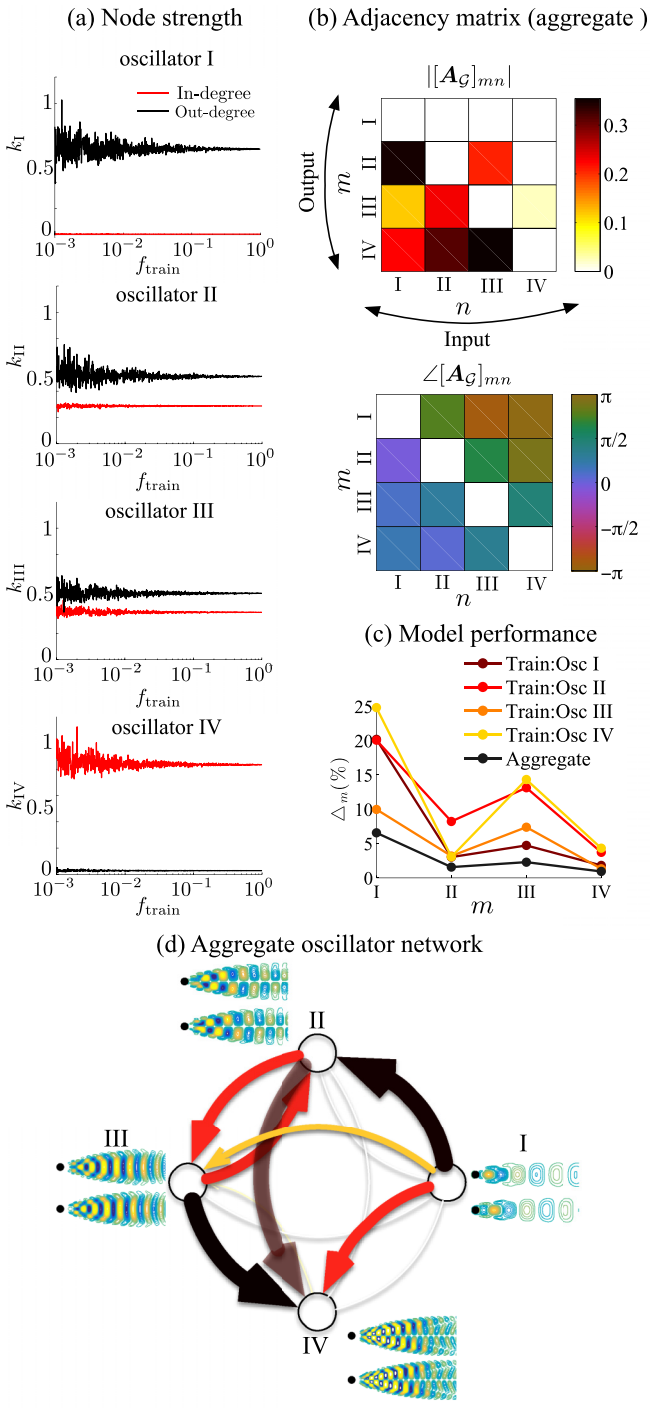

FIG. 5. (a) Network degrees for varying fractions of training data. (b) Adjacency matrix of the aggregate network model and (c) the associated model performance. (d) Aggregate network structure of oscillator interactions. The color and thickness of the edges in the network represent the magnitude of the elements of $\boldsymbol{A}_\mathcal{G}$.

where n_t is the length of the test data set. Here, $\dot{\zeta}_m(k)$ is the time derivative of oscillator m obtained from DNS and $\hat{\dot{\zeta}}_m(k)$ is the predicted time derivative value based on the oscillator network model for the kth test data point. The root mean square deviation is normalized by the range of the measured data. We can observe from Fig. 5(c) that the aggregate model achieves the lowest error level in predicting the normalized fluctuation time derivative. As the aggregate model contains more information of the general interactions based on various oscillator perturbations, it yields enhanced predictive capabilities for energy transfer amongst all oscillators. Thus, the aggregate network structure shown in Fig. 5(d) yields a global oscillator interaction model. For the cylinder flow problem, the passage of energy from lower-order oscillators to the higher-order ones is highlighted. Based on the modal interactions characterized using the aggregate network model, we design flow control strategies to suppress modal fluctuations.

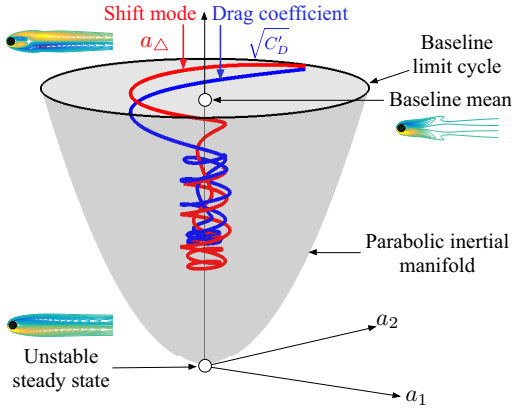

FIG. 6. Shift mode temporal coefficient (red) and drag coefficient (blue) variation (indicated by arrows) with application of control. Parabolic inertial manifold shown in gray.

E. Feedback control

Suppression of modal oscillations is critical in reducing the wake unsteadiness. Roshko [11] and Mao *et al.* [59] reported the strong relationship between unsteadiness in the wake and the drag force acting on the bluff body. As mentioned previously, modal oscillations in the flow are reflected in the temporal coefficients associated with the modes. If the application of control forces the modal temporal coefficients to zero, the flow will approach the mean flow. However, the mean flow is not a steady solution to the Navier-Stokes equation in general, and hence the flow diverges from the mean towards the unstable steady state in this cylinder flow case.

In the seminal work of Noack *et al.* [24], it was shown that the mean flow and the unstable steady state are connected by a shift mode. The shift mode for the cylinder flow problem is shown in Fig. 6 (top left). This shift mode captures the transient dynamics between the onset of vortex shedding near the unstable steady state shown in Fig. 6 (bottom left) and the baseline mean flow of the periodic von Kármán vortex street in the globally stable limit cycle. This evolution takes place along the parabolic inertial manifold shown in gray. The vertical axis represents the change in the temporal dynamics associated with the shift mode with application of control. The drag coefficient also varies between the mean baseline value and the unstable fixed point value. A minimum drag coefficient is attained at the unstable steady state C_D^*, which also gives zero lift force on the cylinder. The kinetic energy associated with the shift mode varies as $a_\triangle^2$ and the drag force on the cylinder

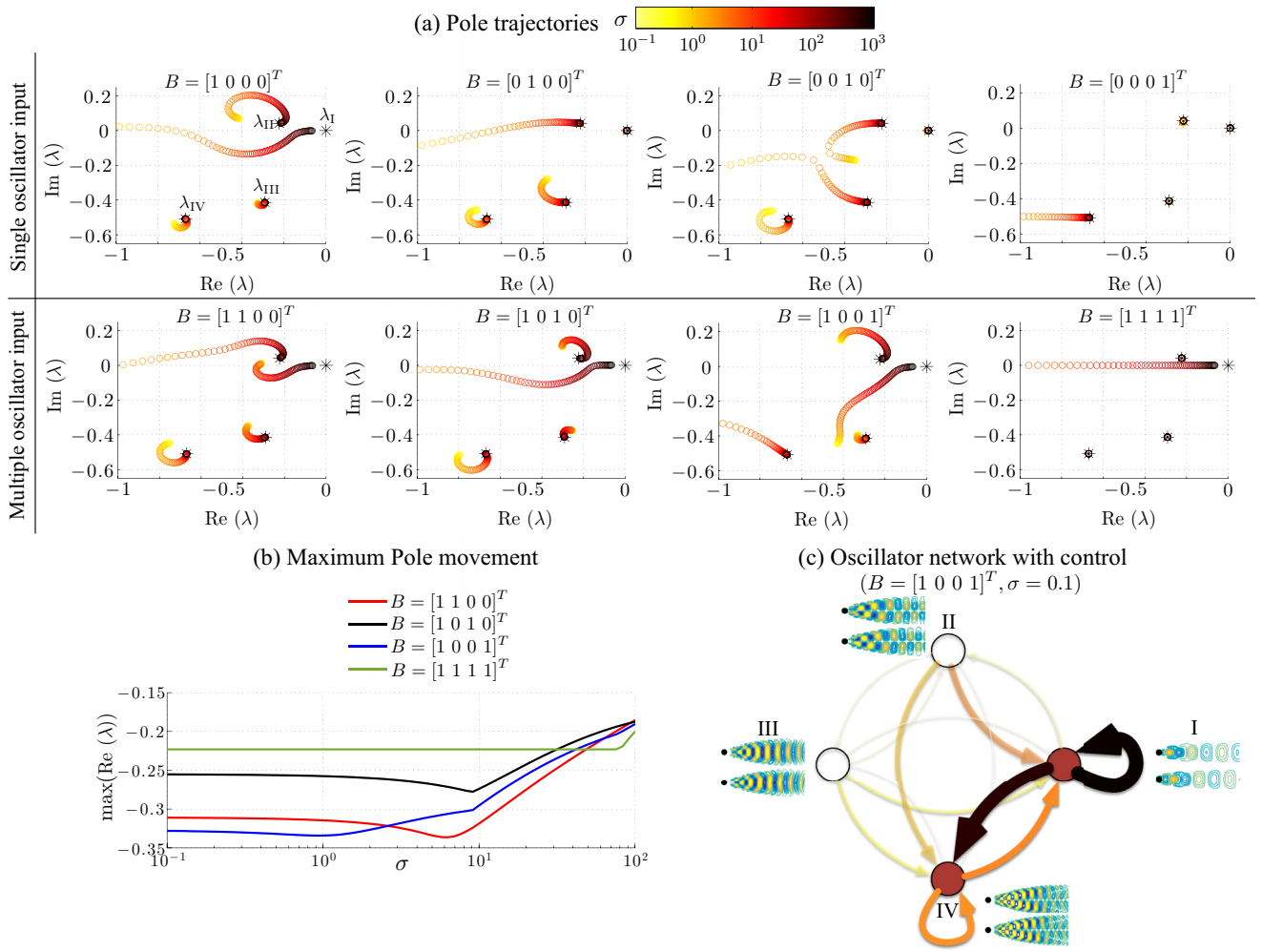

FIG. 7. (a) Pole trajectories with application of different control inputs to the aggregate network model for a range of σ. Stars indicate $\lambda(-\boldsymbol{L}_{\mathcal{G}})$. (b) Movement of max[Re(λ)] for the multiple oscillator input cases. (c) Network structure with control. The oscillators to which control is added are indicated by red (filled) circles. The color and thickness of the network edges in the network represent the magnitude of elements of $(-\boldsymbol{L}_{\mathcal{G}} - \boldsymbol{B}\boldsymbol{K})$.

in the mean shift regime scales as $\sqrt{C'_D} \propto a_{\triangle}$, as shown in Fig. 6 where $C'_D = C_D - C^*_D$. Thus, a mean shift towards the unstable steady state achieves a reduction in drag force.

We first develop a low-dimensional control framework based on the networked-oscillator model to attenuate perturbations in the flow. We then extend the formulation to suppress the overall flow unsteadiness. As the networked-oscillator model given by Eq. (9) is linear, we can exploit the use of the linear quadratic regulator (LQR) to control the modal fluctuations. Adding a forcing input to the networked-oscillator model (in vector form), we arrive at

$$\dot{\boldsymbol{\zeta}} = -\boldsymbol{L}_{\mathcal{G}}\boldsymbol{\zeta} + \boldsymbol{B}\boldsymbol{v}, \tag{15}$$

where $\boldsymbol{\zeta} = [\zeta_{\mathrm{I}}, \zeta_{\mathrm{II}}, \ldots, \zeta_M]^T$, $\boldsymbol{v} \in \mathbb{C}^{M\times 1}$ is the forcing input, and $\boldsymbol{B} \in \mathbb{R}^{M\times 1}$ is the actuation input matrix. The mth entry of $\boldsymbol{B}$ corresponds to forcing being added to oscillator m.

We implement an optimal full-state control with $\boldsymbol{v} = -\boldsymbol{K}\boldsymbol{\zeta}$ such that

$$\dot{\boldsymbol{\zeta}} = (-\boldsymbol{L}_{\mathcal{G}} - \boldsymbol{B}\boldsymbol{K})\boldsymbol{\zeta}, \tag{16}$$

where the gain matrix $\boldsymbol{K}$ is determined from the Riccati equation for LQR. Here, we assume that the POD mode pairs can be used as forcing inputs. While this viewpoint may appear as naive, it provides tremendous insights and guidance in designing localized actuation techniques. An optimal control strategy using LQR minimizes the quadratic cost function of the form

$$J = \int_0^\infty [\boldsymbol{\zeta}(t)^T \boldsymbol{Q}\boldsymbol{\zeta}(t) + \boldsymbol{v}(t)^T \boldsymbol{S}\boldsymbol{v}(t)]dt, \tag{17}$$

where $\boldsymbol{Q}$ and $\boldsymbol{S}$ are the state deviation and input usage weights, respectively. Here, we set $\boldsymbol{Q} = \boldsymbol{I}$ and $\boldsymbol{S} = \sigma\boldsymbol{I}$ and consider a range of values for σ.

We can force the individual oscillators or a combination of oscillators. To aid the selection of which oscillators to force, we examine the movement of the eigenvalues of $\boldsymbol{L}_{\mathcal{G}}$ with control for different combinations of input matrix $\boldsymbol{B}$ as shown in Fig. 7. Eigenvalues of Laplacian matrix $\lambda(-\boldsymbol{L}_{\mathcal{G}})$ reveal the dynamical characteristics of the system. As four oscillators are considered in this paper, we obtain four eigenvalues $(\lambda_{\mathrm{I}}, \ldots, \lambda_{\mathrm{IV}})$ for

varying σ in Fig. 7. Note that $\lambda_m \leqslant 0$ for all eigenvalues which is a characteristic feature of Laplacian-based systems.

We compare the response for input matrix $\boldsymbol{B}$ for both single oscillator input and some multiple oscillator input cases. For each input case, we determine the LQR gain matrix $\boldsymbol{K}$ for values of σ ranging from 0.1 to 1000 and examine the movement of eigenvalues of the operator, $(-\boldsymbol{L}_{\mathcal{G}} - \boldsymbol{B}\boldsymbol{K})$, which govern the behavior of the controlled system. For the single-oscillator input cases, we observe large movement of the eigenvalue corresponding to the forced oscillator as σ is decreased, i.e., the real part of λ_m decreases when more forcing input is provided to oscillator m. We also notice that an input in oscillator I affects all eigenvalues while inputs to the higher-order oscillators do not move the λ_{I} eigenvalue. This is expected as oscillator I has maximum out-degree and correspondingly has the highest influence in the network.

As an input to oscillator I is required to affect the λ_{I} eigenvalue, we consider multiple oscillator input cases including oscillator I. A noticeable movement in the eigenvalues is observed with inputs on oscillators I and IV. For forcing inputs added to all oscillators, only the λ_{I} eigenvalue is affected with no influence on the other system eigenvalues. To summarize the effectiveness of forcing input on controlling the system behavior, we track max[Re(λ)] for multiple oscillator input cases in Fig. 7(b). We observe that for small σ oscillator input combinations of I and IV outperform the other input combinations.

We consider the LQR controller such that system eigenvalues move towards the left side of the complex plane as much as possible. Thus, we select the input matrix $\boldsymbol{B} = [1001]^T$ which adds forcing input to oscillators I and IV. Considering full-state feedback control with this choice of $\boldsymbol{B}$, we compute the control gain matrix $\boldsymbol{K}$ using LQR for a particular σ. Introducing control modifies the interaction between oscillators. We extract this modified network structure of interactions for $\sigma = 0.1$ from the controlled Laplacian $(-\boldsymbol{L}_{\mathcal{G}} - \boldsymbol{B}\boldsymbol{K})$ as shown in Fig. 7(c). We can clearly notice that control added to oscillators I and IV results in self-loops which attenuate their fluctuations. Strong interactions are observed between oscillators I and IV. In addition, we also observe interactions corresponding to transfer of energy from oscillators II and III to oscillators I and IV. The incoming interactions to oscillators II and III are weakened considerably. Thus, energy transfers are concentrated to the oscillators where control is added which are ultimately attenuated due to the forcing resulting in self-loops. In the following discussion, we examine two control scenarios. First, we attenuate modal perturbations introduced in the flow. Then, we apply the LQR-based feedback control to suppress all modal amplitudes altogether.

We first illustrate the control of modal disturbances introduced to the cylinder flow. This entails the control of fluctuations in the modal temporal coefficients (z'_m). To demonstrate the control, we consider random amplitude perturbations added to all oscillators about 2% of respective baseline fluctuations. The temporal coefficients of the oscillators for this perturbed case obtained from DNS are shown in Fig. 8 (left). The networked-oscillator control system given by Eq. (16) describes control of temporal coefficients associated with the modes. To implement control design in DNS, a body force corresponding to $-\boldsymbol{B}\boldsymbol{K}\boldsymbol{\zeta}$ is added to the momentum equation

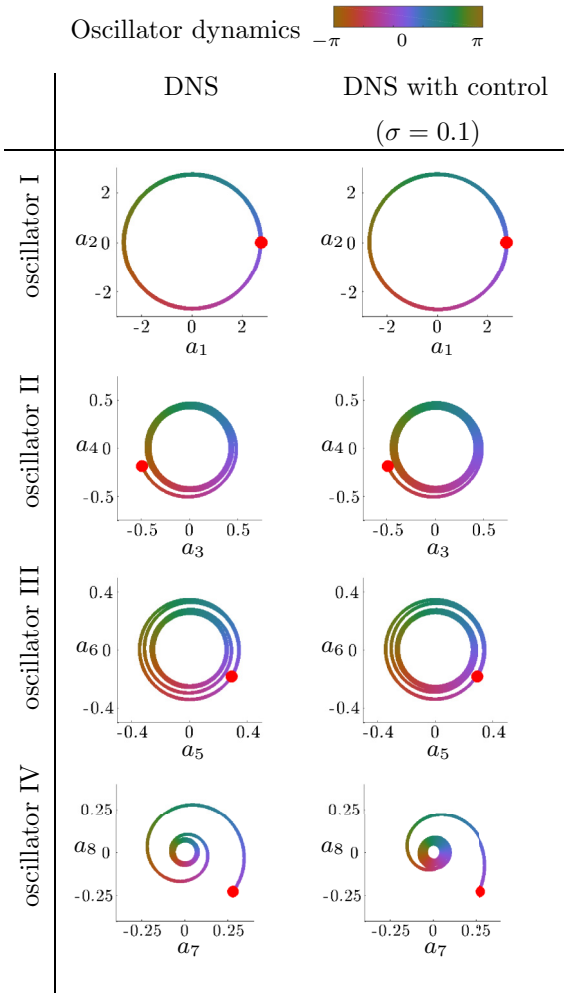

FIG. 8. Oscillator dynamics without control and with control implemented in DNS for suppressing perturbations to the limit cycle.

with the spatial modal information incorporated along with the temporal coefficients. The results with the application of control in DNS for $\sigma = 0.1$ are shown in Fig. 8 (right). We can drive the oscillators to the natural limit cycle much faster with control. We notice that as control is introduced in oscillators I and IV the effectiveness of control is more pronounced with these oscillators. This also follows from Fig. 7 where the correspondence between the Laplacian eigenvalues and oscillator inputs was discussed. Similar analysis can be performed for controlling a variety of modal perturbations introduced.

We then consider the control of total modal oscillations in the flow associated with wake unsteadiness. This requires the control of the temporal coefficients associated with the oscillators (z_m). Though the oscillator interactions characterized in this paper are based on fluctuations with respect to the natural limit cycle (baseline) state, we consider these interactions to be characteristic of the modal oscillations in the flow. In fact, the energy transfer mechanism should be similar for z'_m and $z'_m + z^b_m$. We realize that by suppressing z_m the flow is attracted towards the unstable steady state. Since we can assume that the above networked-oscillator-based LQR control is applicable near the baseline limit cycle, we expect that there is some region

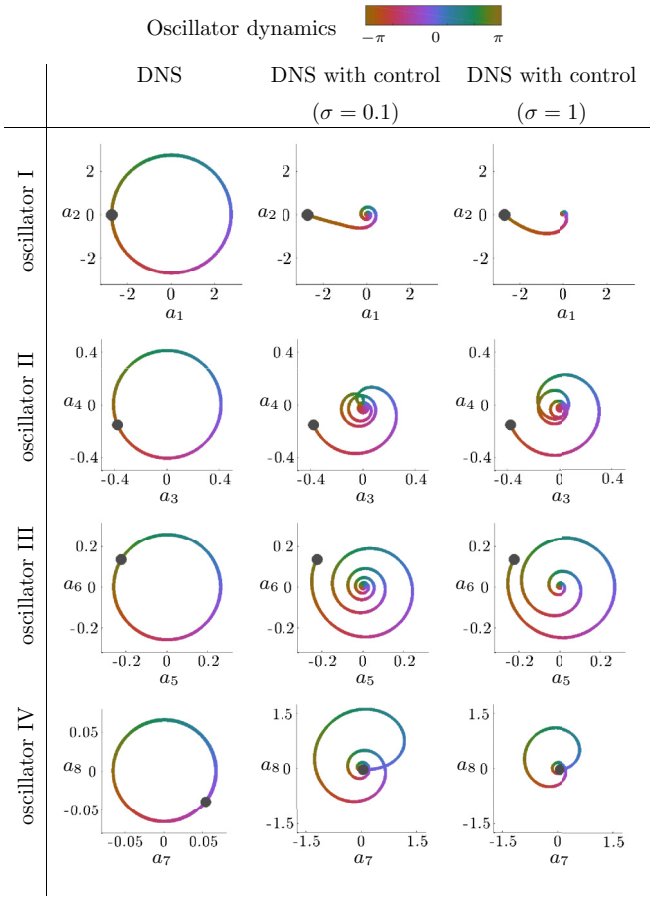

FIG. 9. Oscillator dynamics without control and with control implemented in DNS for suppressing modal oscillations.

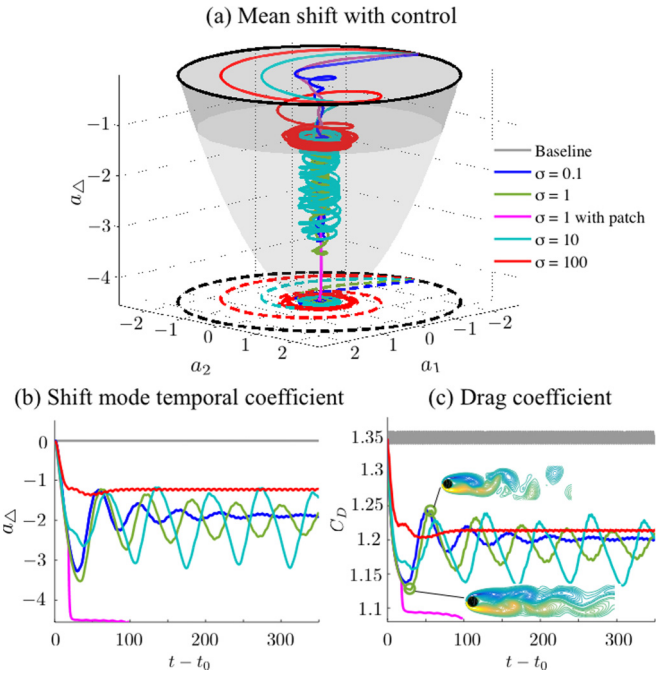

FIG. 10. (a) Shift mode temporal dynamics on the parabolic inertial manifold for a range of σ and (b) shift mode temporal dynamics in the time domain. (c) Drag force compared to the baseline.

of validity of control to achieve drag reduction. Inhibiting nonlinear energy transfer should remove the energy input to sustain wake oscillations. Hence, we expect to use the same aggregate model extracted to suppress the limit cycle along with fluctuations of the modes to some degree.

Our objective is to control the temporal coefficients associated with the modes, yielding a control system of the form

$$\dot{z}_m = -\sum_{n=\mathrm{I}}^{M} [\boldsymbol{L}_{\mathcal{G}} - \boldsymbol{B}\boldsymbol{K}]_{mn} z_n. \tag{18}$$

In DNS, this amounts to adding a body force corresponding to $-\boldsymbol{B}\boldsymbol{K}\boldsymbol{z}$. This control input steers the modal amplitudes corresponding to the baseline limit cycle to zero as shown in Fig. 9(a). Here, we show the control performance for $\sigma = 0.1$ and 1. With control, the temporal coefficient associated with oscillator I first decays to zero followed by the higher-order oscillators. The energy lost by oscillator I is compensated with an initial increase in energy associated with oscillator IV. This is expected as oscillator IV is the most influenced node in the network. This highlights the energy transfers from lower-order to higher-order oscillators. As control input is added to oscillator IV, we suppress the corresponding modal oscillations. Once the modal amplitudes are forced to zero, the flow returns to the mean flow. This is expected as the unsteady flow field is decomposed into mean flow and modal components, so that forcing the modal components to zero reduces the flow to the mean. However, the mean flow is not an equilibrium and a shift in the mean flow is observed as time progresses. This mean flow deformation is attributed to the Reynolds stress generated by the modal fluctuations which modifies the base flow [27]. The change in the base flow leads to a corresponding decrease in modal energy until equilibrium is achieved. In the case of the cylinder flow problem, the flow tends towards the unstable steady state.

The mean shift between the mean flow and the unstable steady state can be described by the shift mode. The temporal coefficient ($a_\triangle$) corresponding to the shift mode ($\boldsymbol{u}_\triangle$) can be obtained by projection as $a_\triangle = \langle \boldsymbol{u} - \bar{\boldsymbol{u}}, \boldsymbol{u}_\triangle \rangle$. We also perform control considering $\sigma = 10$ and 100. The variation of shift mode temporal coefficients with respect to temporal coefficients of the dominant POD modes for the range of σ considered is shown in Fig. 10(a). For reference, the evolution of the flow from unstable steady state to the mean flow that follows a parabolic inertial manifold is shown in gray [24]. The darker gray region of the manifold indicates the region of effective control using the networked-oscillator model. In this region, the nonlinear energy transfers are inhibited to reduce wake oscillations. Thus, in suppressing the modal oscillations, we achieve a mean shift in the flow resulting in drag reduction. For the case corresponding to $\sigma = 1$, we collect velocity snapshots in the time interval between $t = 19.3$ and 80 and perform POD analysis on the controlled data. Considering the first ten additional POD modes for control, we construct a linearized model by curve-fitting the temporal coefficients. Designing an additional controller (patch controller) based on these coefficients, we can force the flow to the bottom of the

manifold corresponding to the unstable steady state shown in magenta ($\sigma = 1$ with patch) in Fig. 10(a).

The temporal dynamics associated with the shift mode is shown in Fig. 10(b). It can be observed that initially $a_\triangle = 0$ in the limit cycle and as control is applied the shift mode temporal coefficient decreases and approaches the unstable steady state. As σ decreases, we achieve a steeper decrease in $a_\triangle$. Examining the long time history of the temporal variation of the shift mode, the choice of lower σ results in low frequency oscillations in $a_\triangle$. These low frequency oscillations are attributed to the exchange of energy between the low and moderate drag states [60]. For control effort corresponding to $\sigma = 100$, a steady state with application of control is achieved more rapidly.

The unsteady forces on the cylinder with application of control compared to the baseline drag variation are shown in Fig. 10(c). The variation in the drag coefficient is similar to the shift mode variation as discussed previously. Almost a 12% reduction in drag is achieved with the application of control. With the addition of the patch controller, the minimum drag state is achieved. The networked-oscillator control framework considered here is based on interactive dynamics of the baseline POD modes and does not include any other modes. We, however, note that the shift mode itself can be incorporated into the controller [47,61].

The unsteady forces on the cylinder can be reduced by suppressing modal oscillations in the flow and inhibiting energy transfers therein. Using a networked-oscillator model in conjunction with optimal control, we can control energy transfer dynamics effectively for unsteady wake flows.

IV. CONCLUDING REMARKS

In summary, we constructed a networked-oscillator model to describe modal interactions in unsteady wake flows. The modal oscillators composed of POD conjugate mode pairs constitute the modal network nodes. The interactions between the oscillators form edges of the network, which were characterized by analyzing impulse responses to the fluid flow. Small perturbations were introduced in the modal oscillators and their transfer of perturbation energy over the network was studied. In the weakly nonlinear limit, the amplitude and phase perturbations introduced in the Navier-Stokes equations were tracked using linear regression to develop the networked-oscillator framework. The networked-oscillator model is a linear approximation to the nonlinear modal interactions in unsteady fluid flows.

Using a canonical example of unsteady flow over a cylinder, the energy transfer dynamics were analyzed. Agreement of the model with DNS was observed for both amplitude and phase perturbation cases. The modal perturbation dynamics is more faithfully captured using the networked-oscillator model compared to the empirical Galerkin formulation. A system identification of impulse responses over a collection of perturbed cases leads to an aggregate network model that captures general oscillator interactions in the flow. The aggregate network model is attributed with the least error in terms of prediction of the temporal dynamics of the modal oscillators. The degree of the nodes corresponding to the aggregate network structure provides insights on the importance of individual oscillators to energy transfers and the overall system dynamics.

With the knowledge of network interactions between oscillators, an optimal feedback control strategy was designed to suppress oscillator fluctuations with respect to the natural limit cycle faster. A judicious choice of the forcing input was made by examining the movement of the poles of the graph Laplacian with LQR. Upon the control of modal disturbances, faster return of modal coefficients to the baseline limit cycle was achieved. Controlling the overall fluctuations of the oscillators resulted in inhibiting energy transfers that sustain wake oscillations and a mean shift towards the (lower energy) unstable steady state. The mean shift correspondingly led to a reduction in the unsteady forces on the cylinder.

The networked-oscillator modeling and control approach shown here leverages the knowledge of modal interactions, providing insights beyond traditional approaches. The embedding of nonlinear dynamics in the linear framework has enabled the design of control strategies based on network structure. The data-driven approach can be extended to more complex flows with broadband modal fluctuations incorporating network models with uncertainty quantification. A stochastic component can also be added to the networked-oscillator model to extend it to flows of increasing complexity involving systems with chaotic limit cycles. Controlling the modal interactions at a fundamental level paves the path for analogous studies using localized actuators and limited sensors for modeling and controlling unsteady fluid flows.

ACKNOWLEDGMENTS

We are grateful for the support by the U.S. Air Force Office of Scientific Research (Grant No. FA9550-16-1-0650; Program Manager, Dr. Douglas R. Smith). We also thank Dr. Bernd Noack for the insightful feedback on modal network based control.

APPENDIX: MODAL INTERACTIONS

The networked-oscillator model of M linearly coupled oscillators is given by Eq. (9). Here, the graph Laplacian is

$$[\boldsymbol{L}_{\mathcal{G}}]_{mn} = \mathrm{diag}\left(\left[\sum_{n=\mathrm{I}}^{M} w_{mn}\right]_{m=\mathrm{I}}^{M}\right) - w_{mn}, \tag{A1}$$

where edge weights are $w_{mn} = |w_{mn}| \exp(i \angle w_{mn}) = |w_{mn}|[\cos(\angle w_{mn}) + i \sin(\angle w_{mn})]$. The interactions between oscillators correspond to the off-diagonal terms of the Laplacian w_{mn}. The normalized oscillator fluctuations can be decomposed into modal fluctuations as

$$\zeta_m = \beta_{2j-1} + i\beta_{2j}. \tag{A2}$$

Here, β_{2j-1} and β_{2j} are the normalized fluctuations of the odd modes ($\boldsymbol{\phi}^{\boldsymbol{u}}_{2j-1}$) and even modes ($\boldsymbol{\phi}^{\boldsymbol{u}}_{2j}$), respectively. The time evolution of the normalized fluctuation of oscillator m is given by

$$\dot{\zeta}_m = \dot{\beta}_{2j-1} + i\dot{\beta}_{2j}. \tag{A3}$$

Substituting Eqs. (A1) and (A2) in Eq. (9), the modal dynamics corresponding to oscillator m is given as

$$\dot{\zeta}_m = -\left[\sum_{n=\mathrm{I}}^{M} w_{mn}\right](\beta_{2j-1} + i\beta_{2j}) + \sum_{n=\mathrm{I}}^{M} |w_{mn}|[\cos(\angle w_{mn}) + i\,\sin(\angle w_{mn})](\beta_{2k-1} + i\beta_{2k}),$$

where $k = 1,2,\ldots,N/2$ corresponds to the respective conjugate mode pairs of oscillator $n = \mathrm{I},\mathrm{II},\ldots,M$.

Thus,

$$\begin{aligned}\dot{\zeta}_m = &-\left[\sum_{n=\mathrm{I}}^{M} w_{mn}\right](\beta_{2j-1} + i\beta_{2j}) + \sum_{n=\mathrm{I}}^{M} |w_{mn}|[\cos(\angle w_{mn})\beta_{2k-1} - \sin(\angle w_{mn})\beta_{2k}] \\ &+ i\{|w_{mn}|[\sin(\angle w_{mn})\beta_{2k-1} + \cos(\angle w_{mn})\beta_{2k}]\}. \end{aligned} \tag{A4}$$

Comparing Eqs. (A3) and (A4), the effect of the odd mode $\boldsymbol{\phi}^{u}_{2k-1}$ on the dynamics of mode $\boldsymbol{\phi}^{u}_{2j-1}$ is determined to be the coupling interaction term $|w_{mn}|\cos(\angle w_{mn})$, the odd-odd mode interaction. Similarly, we see that the even-even mode interactions are given by $|w_{mn}|\cos\angle w_{mn}$ while the odd-even and even-odd mode interactions are provided by $|w_{mn}|\sin\angle w_{mn}$ and $-|w_{mn}|\sin\angle w_{mn}$, respectively, as illustrated in Fig. 1.

[1] Y. Kuramoto, *Chemical Oscillations, Waves, and Turbulence* (Springer, New York, 1984).

[2] S. H. Strogatz, *Nonlinear Dynamics and Chaos: With Applications to Physics, Biology, Chemistry, and Engineering* (Westview Press, Boulder, Colorado, 2014).

[3] Y. Kuramoto, in *International Symposium on Mathematical Problems in Theoretical Physics* (Springer, New York, 1975), pp. 420–422.

[4] A. Pikovsky, M. G. Rosenblum, and J. Kurths, *Synchronization: A Universal Concept in Nonlinear Sciences* (Cambridge University Press, Cambridge, England, 2003).

[5] Y. Kawamura, H. Nakao, K. Arai, H. Kori, and Y. Kuramoto, Phys. Rev. Lett. **101**, 024101 (2008).

[6] Y. Aizawa, Prog. Theor. Phys. **56**, 703 (1976).

[7] R. E. Mirollo and S. H. Strogatz, J. Stat. Phys. **60**, 245 (1990).

[8] Y. Yamaguchi and H. Shimizu, Physica D **11**, 212 (1984).

[9] C. H. K. Williamson and R. Govardhan, Annu. Rev. Fluid Mech. **36**, 413 (2004).

[10] T. Sarpkaya, J. Fluids Struct. **19**, 289 (2004).

[11] A. Roshko, National Advisory Committee on Aeronautics Report No. TN 3169, 1954.

[12] H. Choi, W.-P. Jeon, and J. Kim, Annu. Rev. Fluid Mech. **40**, 113 (2008).

[13] K. Konishi, Phys. Rev. E **68**, 067202 (2003).

[14] A. Sharma and M. D. Shrimali, Phys. Rev. E **85**, 057204 (2012).

[15] K. Taira, S. L. Brunton, S. T. M. Dawson, C. W. Rowley, T. Colonius, B. J. McKeon, O. T. Schmidt, S. Gordeyev, V. Theofilis, and L. S. Ukeiley, AIAA J. **55**, 4013 (2017).

[16] L. Sirovich, Q. Appl. Math. **45**, 561 (1987).

[17] N. Aubry, P. Holmes, J. L. Lumley, and E. Stone, J. Fluid Mech. **192**, 115 (1988).

[18] G. Berkooz, P. Holmes, and J. L. Lumley, Annu. Rev. Fluid Mech. **25**, 539 (1993).

[19] P. J. Schmid, J. Fluid Mech. **656**, 5 (2010).

[20] C. W. Rowley, I. Mezić, S. Bagheri, and D. S. Henningson, J. Fluid Mech. **641**, 115 (2009).

[21] J. N. Kutz, S. L. Brunton, B. W. Brunton, and J. L. Proctor, *Dynamic Mode Decomposition: Data-Driven Modeling of Complex Systems* (SIAM, Philadelphia, PA, 2016).

[22] I. Mezić, Nonlinear Dynamics **41**, 309 (2005).

[23] I. Mezić, Annu. Rev. Fluid Mech. **45**, 357 (2013).

[24] B. Noack, K. Afanasiev, M. Morzynski, G. Tadmor, and F. Thiele, J. Fluid Mech. **497**, 335 (2003).

[25] P. Holmes, J. L. Lumley, and G. Berkooz, *Turbulence, Coherent Structures, Dynamical Systems and Symmetry* (Cambridge University Press, Cambridge, England, 2012).

[26] T. Lassila, A. Manzoni, A. Quarteroni, and G. Rozza, in *Reduced Order Methods for Modeling and Computational Reduction* (Springer, New York, 2014), pp. 235–273.

[27] S. L. Brunton and B. R. Noack, Appl. Mech. Rev. **67**, 050801 (2015).

[28] M. E. J. Newman, *Networks: An Introduction* (Oxford University Press, New York, 2010).

[29] A.-L. Barabási, *Network Science* (Cambridge University Press, Cambridge, England, 2016).

[30] B. Bollobás, *Modern Graph Theory* (Springer, New York, 1998).

[31] E. Otte and R. Rousseau, J. Inf. Sci. **28**, 441 (2002).

[32] X. Zhu, M. Gerstein, and M. Snyder, Genes Dev. **21**, 1010 (2007).

[33] V. J. Wedeen, P. Hagmann, W. I. Tseng, T. G. Reese, and R. M. Weisskoff, Magn. Reson. Med. **54**, 1377 (2005).

[34] P. Hagmann, M. Kurant, X. Gigandet, P. Thiran, V. J. Wedeen, R. Meuli, and J. Thiran, PLoS ONE **2**, e597 (2007).

[35] O. Sporns, Ann. NY Acad. Sci. **1224**, 109 (2011).

[36] S. N. Dorogovtsev and J. Mendes, *Evolution of Networks: From Biological Nets to the Internet and WWW* (Oxford University Press, New York, 2013).

[37] M. Salathé and J. H. Jones, PLoS Comput. Biol. **6**, e1000736 (2010).

[38] K. Robinson, T. Cohen, and C. Colijn, Theor. Popul. Biol. **81**, 89 (2012).

[39] G. Dudas, L. M. Carvalho, T. Bedford, A. J. Tatem, G. Baele, N. R. Faria, D. J. Park, J. T. Ladner, A. Arias, D. Asogun *et al.*, Nature **544**, 309 (2017).

[40] A. G. Nair and K. Taira, J. Fluid Mech. **768**, 549 (2015).

[41] D. A. Spielman and N. Srivastava, SIAM J. Comput. **40**, 1913 (2011).

[42] K. Taira, A. G. Nair, and S. L. Brunton, J. Fluid Mech. **795**, R2 (2016).

[43] M. H. Kutner, C. Nachtsheim, and J. Neter, *Applied Linear Regression Models* (McGraw-Hill, New York, 2004).
[44] H. Kori, Y. Kawamura, H. Nakao, K. Arai, and Y. Kuramoto, Phys. Rev. E **80**, 036207 (2009).
[45] S. Bagheri, J. Fluid Mech. **726**, 596 (2013).
[46] J.-C. Loiseau and S. L. Brunton, J. Fluid Mech. **838**, 42 (2018).
[47] B. R. Noack, M. Morzynski, and G. Tadmor, *Reduced-Order Modelling for Flow Control* (Springer-Verlag, New York, 2011).
[48] K. Taira and T. Colonius, J. Comput. Phys. **225**, 2118 (2007).
[49] T. Colonius and K. Taira, Comput. Methods Appl. Mech. Eng. **197**, 2131 (2008).
[50] T. Kajishima and K. Taira, *Computational Fluid Dynamics: Incompressible Turbulent Flows* (Springer, New York, 2017).
[51] C. Liu, X. Zheng, and C. H. Sung, J. Comput. Phys. **139**, 35 (1998).
[52] D. Canuto and K. Taira, J. Fluid Mech. **785**, 349 (2015).
[53] S. L. Brunton, J. L. Proctor, and J. N. Kutz, Proc. Natl. Acad. Sci. USA **113**, 3932 (2016).
[54] D. Rempfer, Theor. Comput. Fluid Dyn. **14**, 75 (2000).
[55] B. R. Noack, M. Schlegel, B. Ahlborn, G. Mutschke, M. Morzyński, P. Comte, and G. Tadmor, J. Non-Equilib. Thermodyn. **33**, 103 (2008).
[56] B. R. Noack, P. Papas, and P. A. Monkewitz, J. Fluid Mech. **523**, 339 (2005).
[57] I. Akhtar, A. H. Nayfeh, and C. J. Ribbens, Theor. Comput. Fluid Dyn. **23**, 213 (2009).
[58] Y. Gong, Q. Wang, and Z. Wang, Comput. Methods Appl. Mech. Eng. **315**, 780 (2017).
[59] X. Mao, H. M. Blackburn, and S. J. Sherwin, J. Fluid Mech. **775**, 241 (2015).
[60] P. M. Munday and K. Taira, Phys. Fluids **25**, 013601 (2013).
[61] D. M. Luchtenburg, B. Günther, B. R. Noack, R. King, and G. Tadmor, J. Fluid Mech. **623**, 283 (2009).